Received August 20, 2019, accepted October 6, 2019, date of publication November 12, 2019, date of current version December 23, 2019.

Digital Object Identifier 10.1109/ACCESS.2019.2953052

Start-Up Control and Grid Integration Characteristics of 300 MVar Synchronous Condenser With Voltage Sourced Converter-Based SFC

PUYU WANG[1], (Member, IEEE), XING LIU[1], QINGWEN MOU[1], WEI GU[2], (Senior Member, IEEE), AND XUEHUA ZHAO[3]

[1]Department of Electrical Engineering, School of Automation, Nanjing University of Science and Technology, Nanjing 210094, China
[2]Jiangsu Provincial Key Laboratory of Smart Grid Technology and Equipment, Southeast University, Nanjing 210096, China
[3]Maintenance Branch, State Grid Jiangsu Electric Power Co., Ltd, Nanjing, 211100, China

Corresponding author: Puyu Wang (puyu.wang@hotmail.com)

This work was supported in part by the National Natural Science Foundation of China under Grant 51807091, in part by the Natural Science Foundation of Jiangsu Province under Grant BK20180478, in part by the China Postdoctoral Science Foundation under Grant 2019M661846, and in part by the Science and Technology Program of the State Grid Jiangsu Electric Power Company, Ltd., under Grant 5210EC16000Q, and in part by the Jiangsu Provincial Key Laboratory of Smart Grid Technology and Equipment Project.

ABSTRACT Synchronous condenser (SC) is generally used as the devices for reactive power support for the ultra-high-voltage direct current (UHVDC) transmission at the receiving end. When a SC is started, it will have a large surge on the interconnected system and the SC itself. In severe cases, it will endanger the operation of SC and related equipment. The start-up control of a 300 MVar SC using voltage source converter (VSC)-based static frequency converter (SFC) is proposed in this paper. Dynamic behaviors of interconnected system during the start-up period with three different criterions of grid integration constraint of the SC, including initial falling speed, frequency difference and phase difference, are analyzed. Firstly, topological structure and control strategy of the VSC-based SFC are proposed. Secondly, a mathematical model of the SFC-based SC is established. The surge of the start-up and grid integration of the SC with three different constraint criterions on the interconnected system is analyzed in sequence. Thirdly, a simulation system of a 300 MVar SC with VSC-based SFC is established in the time-domain simulation software PSCAD/EMTDC^{TM}. Dynamic behaviors and surge of the overall system with different criterions of grid integration constraint are demonstrated and studied. Finally, a comprehensive starting control strategy of the SC with optimized initial falling speed, optimized frequency difference and optimized phase difference is proposed based on the theoretical analysis and simulation experiments. Simulation results justify the effectiveness of the start-up and grid integration control strategy proposed.

INDEX TERMS Synchronous condenser, voltage source converter (VSC)-based static frequency converter (SFC), start-up and grid integration control, constraint criterions, dynamic behaviors.

NOMENCLATURE

SFC	Static frequency converter
SC	Synchronous condenser
VSC	Voltage source converter
CSC	Current source converter
UHVDC	Ultra-high-voltage direct current
HC	Hierarchical connection
SVC	Static var compensator
LCC	Line commutated converter
IGBT	Insulated gate bipolar transistor
CDPA	compensation depth (%) of phase advance
PWM	Pulse-width modulation
CF	Commutation failure
Δf_i	Frequency difference
$\Delta\delta_i$	Phase difference
ω_0	Initial falling sped
P_i	Surge of active power

The associate editor coordinating the review of this manuscript and approving it for publication was Enamul Haque.

Q_i Surge of reactive power
U_i Surge of terminal voltage
I_i Surge of terminal current

I. INTRODUCTION

With the rapid development of UHVDC transmission technology, long-distance power transmission with bulk capacity has been achieved in many countries [1]–[3]. Applications of HVDC play an important role in transporting affluent wind, solar, and hydro power resources from remote areas to load centers, realizing the inter-supply of power between regions/countries and optimal allocation of resources [4], [5]. However, with the grid integration of HVDC, operation and control characteristics of the whole system become more complex. The stability issues of transient, sub-transient and super-transient need to be considered. In addition, the operation of UHVDC converter stations continuously consumes large amounts of reactive power, which needs sufficient reactive power support at AC side under disturbance/fault conditions particularly. Hence, higher requirements are put forward for large capacity dynamic reactive power compensation devices. Dynamic reactive power compensation devices applied for UHVDC converter station are mainly SCs and SVC. In comparison with SVC, SCs have strong-capability of anti-interference, providing a strong reactive power support in a short period of time. Its reactive power output can be regulated flexibly according to the operating condition of power grid and the need of compensation. Moreover, the ability of the system to resist CF can be improved after system disturbances [6], [7]. However, there is little research on dynamic behaviors of the start-up and grid integration the UHVDC converter station with large capacity SC.

SCs are usually initiated by the SFC with variable slip mode and the interconnected power grid. There are two processes for the start-up and grid integration of SCs. Firstly, the rotor speed of SC is increased to a specified speed by the other-excitation mode. Secondly, the stator voltage is established by switching to the self-excitation mode [8]. The SFC and excitation system cooperate with each other to drag the rotor of SCs to accelerate. After accelerating to the specified/preset speed, the SFC system will be exited operation. The rotor speed of SCs will gradually drop under the load torque. In this process, the synchronization control device is activated to capture the effective instant of interconnection and closing signal is sent to the integration circuit breaker and completion the grid integration [9]. Dynamic performance of the voltage at the machine-end and the grid-side are impacted on the voltage phase, speed change rate and initial speed of the SCs. In grid integration process, the speed of SCs controlled by the electromagnetic torque will convert from the rotor speed of grid integration to the synchronization speed. The system oscillations will become more significant during the grid integration with a larger difference between the rotor speed and the synchronization speed [10]. Dynamic behaviors of grid integration of SCs at different frequency under variable slip mode were analyzed in [11]. The grid integration instant of SCs under the most unfavorable condition was calculated, and the optimized grid integration frequency was proposed. The influence on the falling speed and grid integration of SCs made by mechanical load characteristics and electromagnetic torque was analyzed in [12]. The results indicated that the speed of SCs falls slowly without excitation while that falls fast with excitation. The SC interconnected the LCC-HVDC system was analyzed in [13], it can enhance the ability to resist CF. The advantages and disadvantages at two different start-up schemes with the SFC were considered in [14]. One is that when the rotor speed of SC was accelerated to 95% of the rated speed with variable frequency, the operation of SFC was quit and grid integration of SC was completed. The other is that when the rotor speed of SC with SFC was reached to 105% of the rated speed, the operation of SFC was quit. When the synchronization grid integration constraint criterions were met, the grid integration of SC was completed. However, research has been rarely conducted regarding the criterions of grid integration constraint of SCs with VSC-based SFC, including the initial falling speed, frequency difference and phase difference, which has significant impact on dynamic behaviors of the start-up and grid integration of SC.

Different strategies using SC, synthetic inertia of wind power plant, and their combination were proposed and analyzed to enhance the frequency stability of low-inertia systems under various scenarios and wind conditions in [15]. The combination of SC with automatic voltage regulator hardware-in-the-loop test and synthetic inertia offers a better improvement on both the frequency stability and the system synchronism under various operating conditions. However, the grid integration of SC with different frequency differences was not discussed. The combined effect of VSC-based sources and SCs under grid unbalanced faults considering two groups of VSC fault-ride-through control strategies was investigated in [16]. It aimed to provide an evaluation of the different control strategies and to explore the impact of equipping a SC at the point of common coupling. However, the start-up control of large-capacity SC with VSC-based SFC was not discussed under the different criterions of grid integration constraint. The use of a SC to mitigate CF in HC-UHVDC system was analyzed in [17]. Analysis of the transient performance of HC-UHVDC for single-phase and three-phase to ground faults was investigated. The simulation results indicated that SC could make the HC-UHVDC system less susceptible to CF, which effectively improved fault recovery performance of the overall system and could reduce transient overvoltage when single or multiple converters were blocked. However, the start-up and grid integration control of SC with VSC-based SFC were not analyzed in HC-UHVDC system. A detailed model of UHVDC receiving system, including converter stations, AC power grids, a SC, and a wind turbine, was investigated in [18]. The characteristics of the SC was studied in different dynamic conditions of the power grids, e.g. AC voltage drops and DC bipolar blocking. However, the dynamic behaviors of the interconnected

system with different criterions of grid integration constraints, were not considered. In [19], a coast-down no-load characteristic testing approach and curve conversion method were proposed for a 300 MVar SC. The start-up process for the SC with the SFC under the switching of excitation mode was analyzed. However, the characteristics of start-up and grid integration with different criterions of grid integration constraints were not discussed.

A CSC-based SFC is mostly used to start SC in existing literature. This is due to the fact that the CSC-based SFC can be used for start-up and grid integration control of large-capacity SCs. In practical applications, a VSC-based SFC is often used to start a small/medium-capacity SCs. The capacity of VSC-based power electronic devices, e.g. the IGBT, gradually increases with the constant upgrade and innovation of power electronics technology [20]. Thus, the starting of the large-capacity SCs with VSC-based SFC under variable frequency control mode is inevitable in the future. This paper conducts more in-depth and prospective study regarding the start-up and grid integration of the large-capacity SC.

This paper investigates the start-up control and grid integration characteristics of 300 MVar SC with voltage sourced converter-based SFC with the main contributions given as follows.

- A topological structure and a mathematical model of a VSC-based SFC and control strategy of starting 300 MVar SC are proposed.
- Dynamic behaviors of the interconnected system with three different criterions of grid integration constraint, including initial falling speed, frequency difference and phase difference in the synchronization grid, are analyzed. Surges of the overall system with different criterions of grid integration constraint on the start-up control is investigated.
- A simulation model of 300 MVar SC with VSC-based SFC is established. Based on theoretical analysis and simulation results, a comprehensive start-up scheme for the SC with optimized initial falling speed, optimized frequency difference and optimized phase difference is proposed.

Simulation results in PSCAD/EMTDC^{TM} justify the effectiveness of the proposed start-up and grid integration control strategy.

II. BASIC OPERATION PRINCIPLE OF SYNCHRONOUS CONDENSER

A. OPERATION PRINCIPLE

There are two types of SC rotor: salient pole type and non-salient pole type. The new large capacity SC usually utilizes non-salient pole SC [21]. The operation principles of non-salient pole SC are analyzed as follows. The active power and reactive power of a non-salient pole SC are expressed as

$$P = \frac{E_q U}{x_d} \sin\delta \tag{1}$$

$$Q = \frac{E_q U}{x_d} \cos\delta - \frac{U^2}{x_d} \tag{2}$$

where, E_q is excitation potential of the SC, U is terminal voltage of the SC, δ is the power angle (the angle between E_q and U), and x_d is synchronous reactance.

SCs are one type of synchronous motor under special operating conditions, without mechanical load and prime mover [21]. The active power input/output is zero, and the SC will only input/output reactive power to the grid according to the demand. Hence, the active power output of the shaft of a SC can be approximated to zero and the losses are negligible compared with its rated capacity. It is assumed in this paper that the active power P, the power angle δ and the core losses of SC are approximated to 0. Meanwhile, (2) can be further derived as

$$Q = \frac{E_q U}{x_d} - \frac{U^2}{x_d} = \frac{(E_q - U)\, U}{x_d} \tag{3}$$

When applying generator convention, the vector relationship between voltage and current of the condenser is expressed under synchronous rotating dq coordinate system.

$$\dot{U} = \dot{E}_q - jx_d\dot{I} \tag{4}$$

where, I is the terminal current amplitude of the SC.

(1) Normal excitation operating condition
$E_q = U$, $\Delta\delta = 0°$, $Q = 0$.
(2) Over-excitation operating condition
$E_q > U$, $\Delta\delta = 90°$, export Q_L(inductive reactive power).
(3) Under-excitation operating condition
$E_q < U$, $\Delta\delta = -90°$, import Q_L(inductive reactive power).

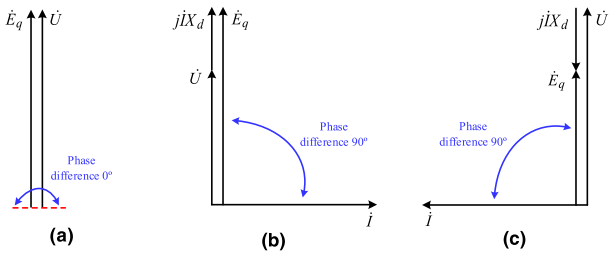

FIGURE 1. The operating vector diagram of synchronous condenser.

The vector diagrams of a SC under different operating conditions are depicted in Fig. 1. When $E_q = U$, i.e. normal excitation operating condition, the phase difference between I and U is 0° and the reactive power output is 0. The vector diagram under normal excitation operating condition is shown in Fig. 1 (a). When $E_q > U$, i.e. over-excitation operating condition, the phase difference between I and U is 90° (I leads U by 90°), the inductive reactive power is exported from the SC. The vector diagram under over-excitation operating condition is shown in Fig. 1 (b). When $E_q < U$, i.e. under-excitation operating condition, the phase difference between I and U is 90° (I lags U by 90°), the inductive reactive power is imported to the SC. The vector diagram under under-excitation operating condition is shown in Fig. 1 (c). Hence,

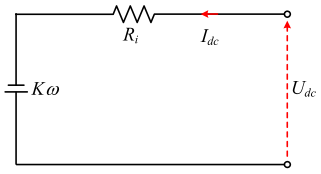

FIGURE 2. Equivalent circuit of SFC system.

the operating modes of the SC can be varied by adjusting the excitation current and thereby achieving the control of reactive power import/export.

B. REACTIVE POWER AND ROTOR SPEED CONTROL

1) REACTIVE POWER CONTROL

(1) Normal excitation operating condition $E_q = U$, $Q_{Nor} = 0$,
where, $E_q = I_f \cdot R_f$.

(2) Over-excitation operating condition
Under over-excitation operating condition, the SC exports inductive reactive power. The reactive power can be derived as [22]

$$I_{f\max} = k_{fm} I_{fN} \tag{5}$$

$$Q_{over} = \lim_{I_f \to I_{f\max}} \frac{(E_q - U)U}{x_d} = \frac{(k_{fm}U - U)U}{x_d} = (k_{fm} - 1)\frac{U^2}{x_d} \tag{6}$$

where, k_{fm} is the strong-excitation coefficient of rotor.

(3) Under-excitation operating condition
Under under-excitation operating condition, the SC imports inductive reactive power. The reactive power can be derived as

$$Q_{under} = \lim_{I_f \to 0} \frac{(E_q - U)\,U}{x_d} = \frac{(0 - U)\,U}{x_d} = -\frac{U^2}{x_d} \tag{7}$$

Hence, the reactive power under different operating conditions can be expressed as

$$Q = \begin{cases} -\dfrac{U^2}{x_d} & U > E_q \\ (k_{fm} - 1)\dfrac{U^2}{x_d} & U < E_q \\ 0 & U = E_q \end{cases} \tag{8}$$

2) ROTOR SPEED CONTROL

Equivalent circuit of the SFC system is depicted in Fig. 2.

Under steady-states the DC current can be derived as

$$I_{dc} = \frac{K\omega - U_{dc}}{R_i} \tag{9}$$

$$K\omega = U_{dc} + I_{dc}R_i \tag{10}$$

where, K is constant value, $U = K\omega$ is output voltage of the SFC, i.e. the terminal voltage of the SC, U_{dc} is the DC voltage, I_{dc} is DC current, R_i is equivalent resistance of the SFC.

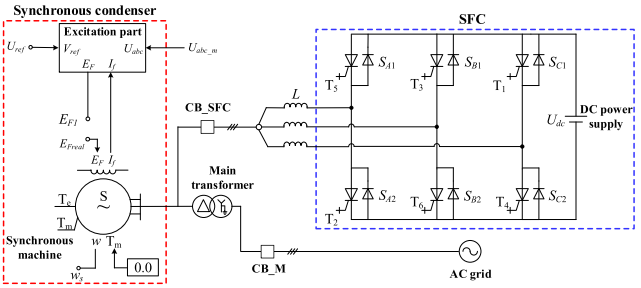

FIGURE 3. Schematic diagram of the SC interconnected AC grid with SFC.

U_q is measured to calculate $K\omega_{t=0}$ which is the output voltage of the SFC.U_q is the q-axis synchronous voltage. $K\omega_{t=0}$ can be derived as [23]

$$K\omega_{t=0} = \frac{U_q}{\sqrt{2}} \cdot \frac{3\sqrt{2}}{\pi} \approx U_q \tag{11}$$

During the speed falling stage, $K\omega_t > 0$ is proportional to the rotor speed. Hence, $K\omega_t > 0$ can be derived as

$$K\omega_{t>0} = \frac{\omega_{act}}{\omega_{rated}} \cdot K\omega_{t=0} \tag{12}$$

where, ω_{rpm} is the actual rotor speed and ω_{rated} is the rated speed.

III. CONTROL MODE OF STARTING SYNCHRONOUS CONDENSER WITH SFC

A. THE TOPOLOGICAL STRUCTURE AND PARAMETERS

In order to study on dynamic performance of start-up and grid integration of SC, a simulation system of 300 MVar SC with VSC-based SFC is established in the time-domain simulation software PSCAD/EMTDC^{TM}. The diagram of the topological structure of the system is illustrated in Fig. 3. The SFC is depicted in the blue dotted-line frame, including a three-phase six-bridge inverter circuit consisted of fully-controlled power electronics device and a DC power supply. The SC, including excitation part and synchronous machine, is connected to the SFC via SFC connection circuit breaker (CB_SFC). The AC grid is connected to the SC via integration circuit breaker (CB_M) and main transformer.

Inertia is defined as the resistance of a physical object to changes in its state and position, consisting of its speed and direction. The inertia of a power system is referred to the nominal apparent power of synchronous machines. The inertia is inherent in a SC, because it is a synchronous rotating machine operating as a motor with no mechanical load [15]. Since the SC is a rotating device, it can provide inertia for the system resulting its active power exchange with the grid during the transients. According to the operating characteristics and published literature regarding synchronous machines, the inertia of a SC is generally selected in the range of 2.0∼6.0 MWs/MVA [24]. In this paper, the inertia is selected at 3.0 MWs/MVA.

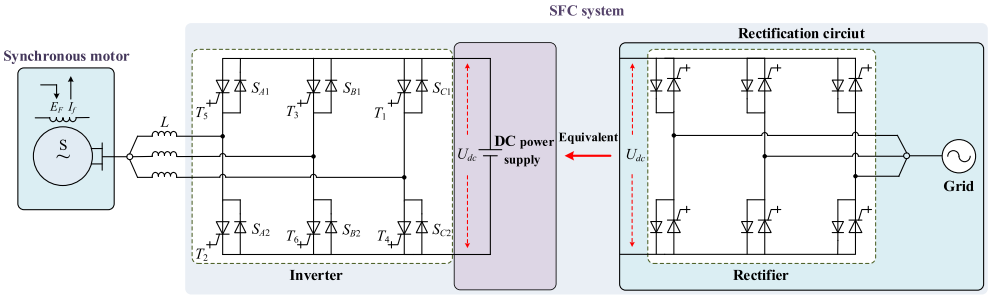

FIGURE 4. Topological structure of a rectification circuit to generate the DC power supply.

TABLE 1. Parameters of the SC Interconnected AC Grid with SFC.

Parameter	Value
Capacity of transformer	360 MVA
AC system nominal voltage	500 kV
Nominal DC voltage of the converter	10 kV
Nominal DC current of the converter	0.5 kA
Transformer ratio	500 kV/20 kV
SC capacity	300 MVar
Compensation depth of phase advance	-150 MVar
Rotor speed	3000 r/min
Stator voltage	20 kV
Stator current	8.66 kA
Frequency	50 Hz
Inertia constant	3.0 MWs/MVA
Mechanical friction	0.01 p.u.

Mechanical friction (also known as mechanical damping) is a portion of the machine rated torque. The mechanical damping friction in per-unit can be derived as [24]

$$D_{pu} = D_m \cdot \frac{(2\pi f)^2}{P_i} \tag{13}$$

where, D_m is the mechanical friction constant in metric, D_{pu} is the mechanical friction constant in per-unit, P_i 3-phase rating power of the synchronous machine. The input of mechanical friction constant is typically between 0 and 0.05 (0 means no frictional losses). The mechanical friction is selected as 0.01 p.u. in this paper. The system parameters are given in Table 1.

The VSC provides the variable-frequency voltage by converting a DC voltage. The DC voltage is generally obtained from an AC rectification. In order to explain the nature of the DC power supply, a topological structure of a rectification circuit to generate the DC power supply is illustrated in Fig. 4. The DC power supply shown in Fig. 4 is generally obtained from a rectification circuit, which can be simplified as a DC voltage source.

B. THE START-UP CONTROL STRATEGY WITH THE VSC-BASED SFC

1) START-UP CONTROL

The core of the start-up control system for the SC is SFC, which provides variable adjustable frequencies at its AC terminal at the initial stage. Currently, three main types of SFC techniques are generally applied, including DC current thyristor control, DC voltage chopper control, and pulse width modulation control [25], [26]. The conventional SFC uses the CSC-based, which adjusts the frequency by controlling the turn-on/turn-off of thyristor, this is due to the fact that the CSC-based SFC can be utilized for the start-up and grid integration of large-capacity SCs. However, the VSC-based SFC is used for the start-up and grid integration of small-capacity SCs. Owing to the development of power electronics technology, the VSC-based SFC has become a reality. In this paper, the VSC-based SFC is applied to invert the DC voltage into AC voltage connected to the AC-terminal of SC. The AC voltage frequency with the VSC-based SFC can be adjusted by the variable frequency starting control mode, to gradually increase to 52.5 Hz. The rotor speed increases with the growth of the AC-terminal voltage frequency. When the rotor speed has reached 105% of the rated speed, the CB_SFC is disconnected. The SC goes into falling speed operating condition. When the criterions of grid integration constraint for the SC, including the frequency difference, voltage phase difference and voltage difference, are met, it will be interconnected the system.

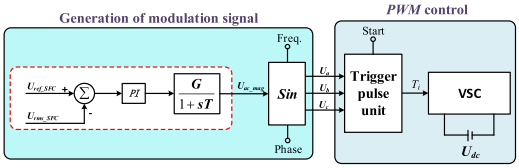

FIGURE 5. Block diagram of the VSC control.

2) THE VSC CONTROL

The VSC-based SFC comprises and is regulated by fully-controlled power electronics device, IGBT. Specifically, the VSC-based SFC can achieve the control of the voltage frequency at the machine-end by fast PWM. Due to the fact that the rotor speed ω of SC is proportional to the input AC voltage frequency, ω can be adjusted by controlling the voltage frequency through the control of the SFC. In order to explain the operating condition of the VSC more clearly, a block diagram of the VSC control is depicted in Fig. 5. Initially, the trigger pulse unit is initiated by sending a starting command. The voltage reference (U_{ref_SFC}) and voltage measurement (U_{rms_SFC}) at the inverter-side of CB_SFC is

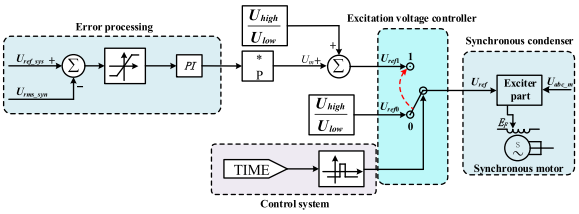

FIGURE 6. Excitation control of synchronous condenser.

compared. The comparison error then passes through a *PI* controller and a filter to obtain the amplitude of the modulation signal (U_{ac_mag}). The trigger voltage U_i ($i = a, b, c$) are sent to the trigger pulse unit to generate the gate trigger signal T_j ($j = 1, 2, 3, 4, 5, 6$). The VSC is initiated by the T_j.

C. EXCITATION CONTROL

In order to explain the excitation control characteristic of the SC, a control diagram is depicted in Fig. 6. The voltage reference (U_{ref_sys}) and voltage measurement (U_{rms_sys}) at the left side of the CB_M is compared, the comparison error then passes through a limiter and a *PI* controller to obtain the amplitude of the error signal (U_m). The U_m and main transformer ratio (U_{high}/U_{low}) is compared to obtain the output voltage ($U_{ref\,1}$). Initial start-up boost stage and variable frequency starting stage, the tap of excitation voltage controller is placed at 0 and the output voltage is $U_{ref\,0}$. When the CB_SFC is disconnected, the control system will send a starting command to change the tap of excitation voltage controller to 1 and the output voltage becomes $U_{ref\,1}$. Hence, the output voltage (U_{ref}) and the voltage (U_{abc_m}) at right side of the CB_M are generated to the exciter part.

D. START-UP AND GRID INTEGRATION CONTROL SEQUENCE

It should be indicated that in order to ensure successful rates of the integration of the SC, the processes of start-up and grid integration following the precise the control sequence is essential. Thus, the control sequence is as follows.

- **Step 0:** Initially, the SC is in static mode and the SFC is blocked;
- **Step 1:** Deblock the VSC-based SFC inverter to control the SFC AC-side voltage;
- **Step 2:** The excitation part is activated;
- **Step 3:** The CB_CFC is connected
- **Step 4:** The variable-frequency control is activated and applied on the SFC to gradually increase the frequency of the SC import voltage;
- **Step 5:** When the rotor speed of SC rises to 105% of the rated speed, the CB_SFC is disconnected;
- **Step 6:** Detect the frequency difference, voltage phase difference and voltage amplitude difference of the integration circuit breaker at two sides when the SC goes into falling speed operating condition;
- **Step 7:** When the synchronization constraint criterions are met, the SC is connected into the system by the CB_M.

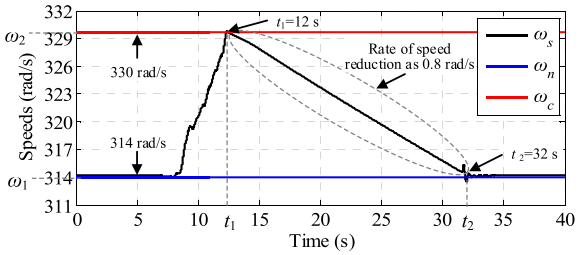

FIGURE 7. Dynamic performance of rotor speed with variable frequency starting control.

It is essential to meet the following conditions for grid integration of SC [27].

(1) The frequency of the system at the interconnection point and that of SC during falling speed process meet the allowable deviation settings value.
(2) The voltage amplitude of the SC and that of the system at the interconnection point meet the allowable deviation settings value.
(3) The voltage phases of the SC and that of the system at the interconnection point meet the allowable deviation settings value.
(4) The voltage phase sequence of the SC is the same as that of the system at the interconnection point.

If the criterions of grid integration constraint are not satisfied, a loop current may be formed between the SC and the power grid, it may enable the stator windings deformed and result in significant damages of the SC. In extreme cases, high-order harmonic loop currents may be formed resulting in a beat vibration current/voltage and the power oscillations of SCs [28].

E. THE START-UP CONTROL CHARACTERISTICS

Prior to the grid integration, when the AC voltage frequency gradually rises to 52.5Hz, the CB_SFC is disconnected and the SC goes into falling speed operating condition. The frequency difference between the SC and the AC system at the interconnection synchronization window is gradually reduced. The voltage phase difference between the SC and the AC system at the interconnection synchronization window is varied between 0 and 360°. When the frequency difference and voltage phase difference between the SC and the system at the interconnection point are less than the setting constraint criterions, i.e. meeting the synchronization constraint criterions, completing the grid integration of the SC.

The SC frequency gradually rises from 0 Hz to 52.5 Hz during the variable frequency starting control stage, i.e. the rotor speed has reached 1.05 times of the rated speed. In this paper, the performance of the grid integration under different constraint criterions are emphatically studied when the rotor speed rises to 1.05 times of the rated speed with variable frequency starting control. It is assumed that the rotor speed of SC has been reached rated speed before deblocking the VSC-based SFC inverter. Dynamic performance of the rotor speed with variable frequency starting control is shown in Fig. 7.

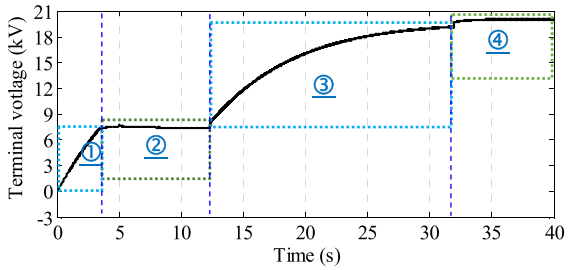

FIGURE 8. Dynamic performance of terminal voltage with variable frequency starting control.

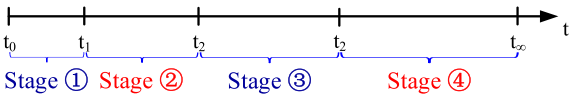

FIGURE 9. Terminal voltage stages control with variable frequency starting control.

Dynamic performance of the terminal voltage under variable frequency starting control is displayed in Fig. 8. Control diagram of terminal voltage is shown in Fig. 9. In this paper, the processes of start-up and grid integration of the SC with SFC are divided into four stages:

- Stage ① : The excitation system is activated at 0s. The terminal voltage rises under the action of self-excitation system, the initial start-up is completed. The SFC is in the blocked-state.
- Stage ② : The SFC is deblocked at 8s, it is indicated that the variable frequency starting control is activated. With the control of SFC, the terminal voltage frequency of SC is regulated to gradually increase from 50 Hz. The amplitude of terminal voltage keeps constant during the variable frequency control.
- Stage ③: When the frequency rises to 52.5 Hz at 12.5s and rotor speed reaches to 1.05 times of the rated speed (3150 r/min), the CB_SFC is disconnected. The rotor speed starts falling speed under the action of load torque. The voltage of the stator is established by the self-excitation system. Moreover, the synchronization device is activated.
- Stage ④: The SC is connected into the system at 32 s, when the frequency difference and phase difference between the SC and the system at the interconnection point meet synchronization constraint criterions, which remains rated terminal voltage stability operation.

In addition, the rate of speed reduction of the rotor can be calculated as

$$\omega_{rate} = \left|\frac{\Delta\omega}{\Delta t}\right| = \left|\frac{\omega_1 - \omega_2}{t_1 - t_2}\right| \tag{14}$$

where, ω_{rate} is the rate of speed reduction of the rotor, $\Delta\omega$ is speed difference, Δt is time difference between t_1 and t_2, ω_1 is the speed at t_1, ω_2 is the speed at t_2. Hence, it can be seen in Fig. 7 that the rate of speed reduction of the SC is 0.8 rad/s.

The start-up control scheme of the SC with VSC-based SFC is consistent with practical engineering. The VSC-based/CSC-based SFC is used to control the AC voltage/current frequency, so that the rotor speed increases with the terminal voltage frequency. When the rotor speed is close to the initial falling speed, the CB_SFC is disconnected. When the synchronization constraint criterions are satisfied during the falling speed, the grid integration of SC is completed.

TABLE 2. The performance with different initial falling speeds.

ω_0 /p.u.	P_i /MW	Q_i /MVar	V_i /kV	I_i /kA
1.01	97.4	550.48	19.98	22.18
1.02	93.9	326.65	20.00	11.96
1.03	100.6	175.81	19.98	8.31
1.04	127.2	100.04	19.91	5.95
1.05	101.1	51.34	19.88	3.71

IV. THREE DIFFERENT CRITERIONS OF GRID INTEGRATION CONSTRAINT

In this section, the different criterions of grid integration constraint of the SC will be analyzed and compared, including different initial falling speeds (ω_0), different frequency differences (Δf) and different phase differences ($\Delta\theta$). The particular conditions of each test case are as follows.

- In order to analyze the grid integration with different initial falling speeds, the frequency difference is set to 0.4 Hz and the phase difference is set to 5°.
- In order to analyze the grid integration with different frequency differences, the initial falling speed is set to 1.05 times of the rated speed and the phase difference is set to 5°.
- In order to analyze the grid integration with different phase differences, the initial falling speed is set to 1.05 times of the rated speed and the integration frequency difference is set to 0.4 Hz.

The dynamic behaviors of active power, reactive power, terminal voltage and terminal current will be emphatically analyzed.

A. GRID INTEGRATION WITH DIFFERENT INITIAL FALLING SPEEDS

When the reactive power load of SC is 0 MVar, the grid integration operation is completed at different initial falling speeds. When the rotor speed of SC rises to 1.01∼1.05 times of the rated speed, the CB_SFC is disconnected and the SC falls into synchronization speed to complete the grid integration operation. The performance of the integration of the SC with different initial falling speeds is presented in Table 2. The frequency difference is set to 0.4 Hz and the phase difference is set to 5°.

It can be seen from Table 2 that when the initial falling speed is $\omega_0 = 1.05$, the surge of the grid integration of SC is the lowest. In addition, according to the simulation results presented in Table 2, the characteristic curves of the falling

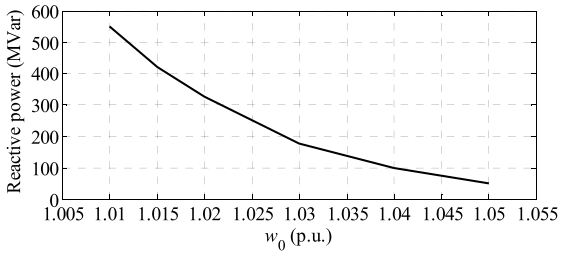

FIGURE 10. Fitted characteristics of ω_0 and surge of reactive power.

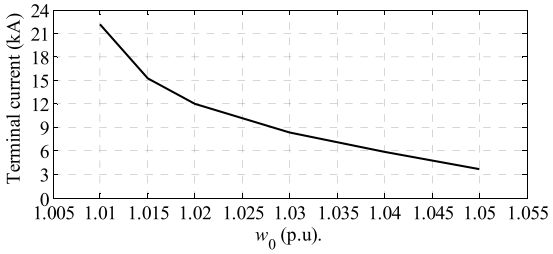

FIGURE 11. Fitted characteristics of ω_0 and surge of terminal current.

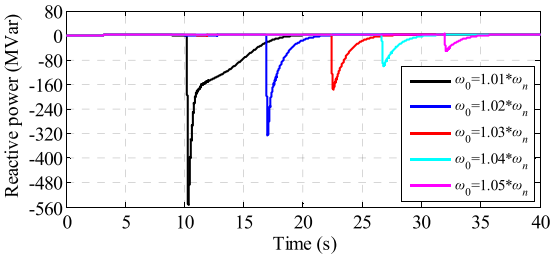

FIGURE 12. The reactive power of synchronous condenser.

speeds and the surges of reactive powers can be fitted as shown in Fig. 10. Based on the fitted characteristic curves, the mathematical relationship is proposed as

$$Q = 250000\omega_0^2 - 527500\omega_0 + 278250 \tag{15}$$

where, Q is surge of reactive power, ω_0 is initial falling speed, and $\omega_0 \epsilon$ (1.01, 1.02, 1.03, 1.04, 1.05).

Similarly, the characteristic curve of initial falling speeds and the surges of terminal currents is fitted as shown in Fig. 11. Based on the fitted characteristic curve, the mathematical relation is proposed as

$$I = 1150\omega_0^2 - 3036\omega_0 + 1924 \tag{16}$$

where, I is surge of terminal current.

The SC, as a dynamic reactive power compensation device, it mainly realizes the control and support of voltage through the outputting/absorbing of reactive power at integration point when the disturbance occurs on the system. The SC makes small contribution to the compensation and control of active power. Hence, the dynamic behaviors of grid integration, including the reactive power, terminal voltage and terminal current, excluding active power are analyzed in this section.

When the SC rises to different initial falling speeds, the CB_SFC is disconnected. The surges of reactive powers of SC with different initial falling speeds are observed

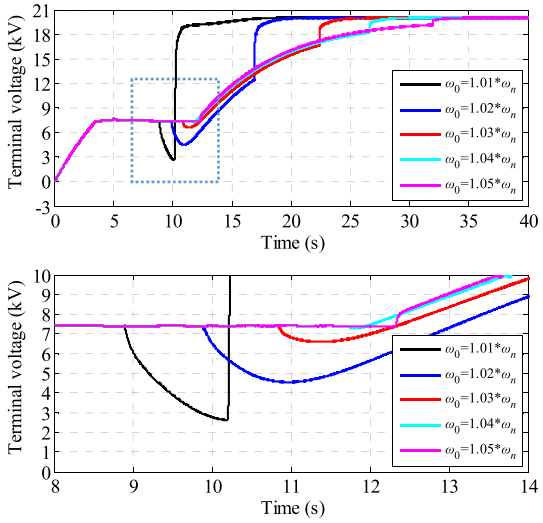

FIGURE 13. The terminal voltage of synchronous condenser.

in Fig. 12. When the initial falling speed is set to 1.05 times of the rated speed, the surge is the lowest. However, when the initial falling speed is set to 1.01 times of the rated speed, the surge exceed over 500 MVar, which is equivalent to 3.67 times of the CDPA. Meanwhile, the setting a smaller speed as the initial falling speed may result in the synchronization window becoming narrower. It may lead to the failure of grid integration when the CB_M cannot detect the appropriate synchronization integration window.

The surges of terminal voltages with different initial falling speeds are presented in Fig. 13. When the initial falling speed of SC rises to 1.01 times of the rated speed, the CB_SFC is disconnected. The voltage of the stator is established during the process, the terminal voltage of SC goes down 67% at 10.2s, and then rapidly rises to the rated voltage. When the falling speed of SC is 1.05 times of the rated speed, the terminal voltage rises smoothly to rated voltage and there is not a fast dropping or a fast rising in a short period of time. Therefore, Fig. 13 persents that when the falling speed of SC is 1.01∼1.03 times of the rated speed, the stator voltage has fast decreases/rise in a short period of time. It may lead to a large surge for the SC and even damage itself. When the initial falling speed of SC is 1.04 or 1.05 times of the rated speed, the terminal voltage rises smoothly, which no have a negative impact on the operation of the SC.

The surges of terminal currents of with different initial falling speeds are presented in Fig. 14. The surge of the terminal current is the lowest when the SC utilizes 1.05 times of rated speed as initial falling speed. When the initial falling speed of SC rises to 1.01 times of the rated speed, the surge peak of the transient over-current reaches to 22 kA, which is equivalent to 2.54 times of the rated current. It will inevitably significant damages for the SC and the low-voltage side of main transformer. Hence, the setting of a lower initial falling speed leads to the emergence of an earlier grid integration instant and a shorter selection range of grid integration, which thereby results in a narrower synchronization window and

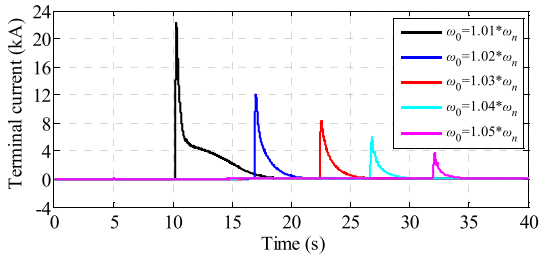

FIGURE 14. The terminal current of synchronous condenser.

finally fewer opportunities for successful grid integration actions.

When the initial falling speed is 1.03 times of the rated speed, it may lead to excessive surges and then relay protection operation. Thus, in comparison with the optimized initial falling speed (1.05 times of the rated speed), an error more than 2% may lead to failure of the grid integration. In the following sections, the performance of grid integration of SC with different frequency difference and phase difference will be compared and analyzed, where the initial falling speed of SC is set to 1.05 times of the rated speed.

B. GRID INTEGRATION OF SC WITH DIFFERENT FREQUENCY DIFFERENCES

When the synchronous condenser begins falling speed, the stator voltage is gradually established. In addition, the synchronization device is activated to capture synchronization integration point. In order to select a closing instant in synchronization window for the integration circuit breaker, three criterions of grid integration constraint must be taken into account. The following three criterions regarding the integration circuit breaker should be met: (1) the frequency difference satisfies the preset range; (2) the phase difference fulfills the defined scale; (3) the difference of the voltage amplitude meets the specified scope. Dynamic behaviors of grid integration under different frequency differences are studied in this section. Generally, the surges of active power, reactive power, terminal voltage and terminal current will be more significant with a larger frequency difference during the grid integration. Table 3 shows that the performance of the SC when the SC is connected into the AC grid power under different frequency difference. Where the phase difference of grid integration point is set to 5° and voltage difference is within 5% [29].

Considering the rotating inertia of SC, the hysteresis of booster transformer and excitation system, the frequency difference of the SC is set larger than 0.3 Hz to ensure the successful rate of grid integration. When the frequency difference is 0.2 Hz or less than 0.2 Hz, the SC cannot capture the grid integration instant to meet constraint criterions in synchronization window, leading to failure of grid integration of the SC. Thus, the criterion of grid integration constraint be set larger than 0.3 Hz. Although the grid integration of the SC can be completed, the instantaneous surges of active power, reactive power and terminal current have a significant

TABLE 3. The performance of SC with different frequency differences.

Δf_i /Hz	P_i /MW	Q_i /MVar	U_i /kV	I_i /kA
0.1	fail	fail	fail	fail
0.2	fail	fail	fail	fail
0.3	101.14	51.34	19.87	3.71
0.4	101.14	51.34	19.92	3.71
0.5	101.14	51.34	19.88	3.71
0.6	184.27	71.26	19.96	7.92
0.7	184.27	71.26	19.91	7.92
0.8	239.54	87.80	19.92	9.43
0.9	239.54	87.80	19.92	9.43
1.0	282.72	103.56	19.92	10.14

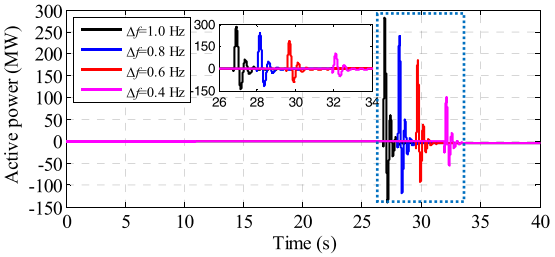

FIGURE 15. The active power of synchronous condenser.

increase when the frequency difference is set to 0.6 Hz ∼ 1 Hz. Therefore, in order to ensure enough the synchronization integration window and appropriate integration control margin and higher successful rate of grid integration, the constraint criterion of integration frequency difference of SC is set to 0.4 Hz ∼ 0.5 Hz.

The surges of active powers of SC under different frequency differences constraint criterions are shown in Fig. 15. Owing to different frequency differences of the grid integration, there is a difference in the grid integration instant. The integration of the SC has more opportunities of capturing the synchronization point and has a higher successful rate with a more relaxed criterion of the frequency difference. However, the surge of active power will become more significant with a larger setting value of frequency difference, which also results in an earlier emergence of the synchronization point. It can be demonstrated in Fig. 15 that when the frequency difference is set to 1 Hz, the surge of active power is the highest, where the surge peak exceeds 280 MW. When the frequency difference is set to 0.4 Hz, the surge of active power is the lowest, where the surge peak is about 100 MW. In comparison with that the constraint criterion is 1 Hz, the surge of active power is reduced by 36%.

The surges of reactive powers of the SC under different frequency differences constraint criterions are shown in Fig. 16. Similarly, the surge of reactive power will become more significant during grid integration with a larger frequency differences between the system side and the SC side. It can be observed in Fig. 16 that when the frequency difference is 1 Hz, the peak surge of reactive power exceeds 100 MVar which is 67% of the CDPA. However, when the frequency difference is 0.4 Hz, the surge peak of reactive power is only 51 MVar which is about 34% of the CDPA.

The surges of terminal voltages of SC under different frequency differences constraint criterions are illustrated

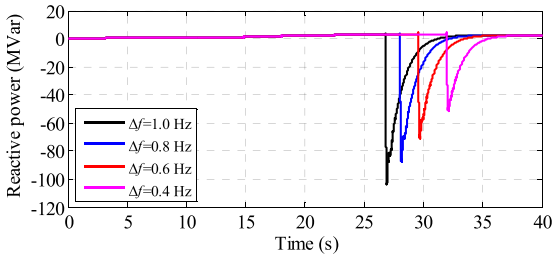

FIGURE 16. The reactive power of synchronous condenser.

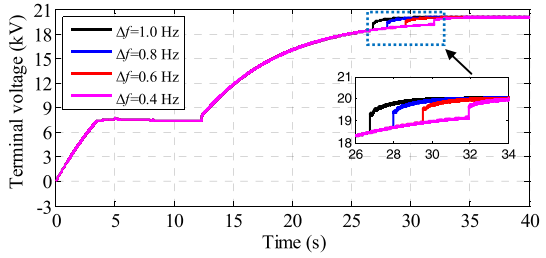

FIGURE 17. The terminal voltage of synchronous condenser.

in Fig. 17. Generally, it is required that the terminal voltage difference of SC is less than 5% of the rated voltage, i.e. the terminal voltage difference of SC is required to be less than 1 kV in this model. It can be seen in Fig. 17 that when the SC is integrated into the system with a larger frequency difference, the terminal voltage difference before/after closing the integration circuit breaker has more significant increase. When the frequency difference is 1 Hz, the terminal voltage is 1.56 kV, which exceeds 50% of the preset value and fails to meet setting value requirements. However, when the frequency difference is 0.4 Hz, the terminal voltage difference is 0.84 kV, which is less than the preset 5% of the rated voltage.

The surges of terminal currents of SC under different frequency differences constraint criterions are shown in Fig. 18. It is generally required that the surge peak value of terminal current at the grid integration instantaneous should not exceed rated current. When the frequency difference of grid integration is set to 0.4 Hz, the surge peak of terminal current is the smallest, which is over 3.7 kA with about 43% of the rated current. However, when the frequency difference of grid integration is set to 0.1 Hz, the surge of terminal current is the highest and the surge peak is over 10 kA, which exceeds the rated value of terminal current. The peak value of transient overcurrent is 1.15 times of the rated current, which does not satisfy the constraint criterion of grid integration.

The simulation results demonstrated that when the frequency difference constraint criterion is set too small, which will result in a narrower synchronization integration window in the speed falling process, it may fail for the grid integration of condenser synchronous. When the frequency difference constraint criterion is set too large, although the grid integration can success, the instantaneous current surges become significant due to a larger frequency difference. It may result in significant damages of the SC and endanger the security

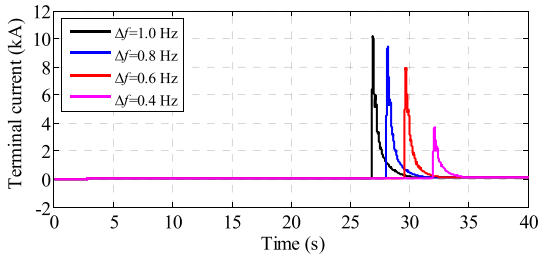

FIGURE 18. The terminal current of synchronous condenser.

TABLE 4. The performance of SC with different phase differences.

$\Delta\delta_i$ / °	P_i /MW	Q_i /MVar	U_i /kV	I_i /kA
1	85.53	50.03	19.86	3.31
2	87.82	50.26	19.90	3.32
3	90.97	50.57	19.88	3.42
4	96.01	50.95	19.87	3.52
5	101.13	51.34	19.92	3.71
6	106.54	51.82	19.89	3.93
7	113.37	52.33	19.94	4.16
8	120.53	52.89	19.91	4.33
9	127.59	53.44	19.92	4.54
10	134.78	54.06	19.93	4.74
10	134.78	54.06	19.93	4.74

and reliability of the system. When the frequency difference is 0.2 Hz or less, it may lead to a narrow synchronization integration window and is possible to not capture a suitable integration instant. In comparison with the optimized frequency difference (0.4 Hz), when the error exceeds 50%, it may lead to failure of the grid integration. Therefore, according to the simulation analysis, in order to ensure the security and stability of grid integration, the frequency difference constraint range is controlled within 0.4 Hz $\sim$ 0.5 Hz.

C. GRID INTEGRATION OF THE SC WITH DIFFERENT PHASE DIFFERENCES

Based on the analysis of the initial falling speeds and the integration frequency differences in Sections IV-A and IV-B, the initial falling speed is set to 1.05 times of the rated speed and the integration frequency difference is set to 0.4 Hz in this section to discuss the integration phase difference of SC. A large amount of power loads are inductive loads in the power grid, such as the motors and transformers. Hence, there must be a phase difference between the voltage and current in the transmission line [30]. Meanwhile, if the phase difference is too large, there will be a torque of the rotor, which may result in permanent damages of the SC [31], [32]. In order to ensure the security and reliability of the SC, the phase difference constraint criterion is studied. The performance of the SC interconnected into the AC grid power with different phase differences is presented in Table 4.

Table 4 shows that when the phase difference constraint criterion of the SC is set between 1° and 9°, the grid integration can be completed normally with a lower surge. In order to ensure the security and stability of grid integration and consider enough control margin, the phase difference is set between 4.5° and 5.5°.

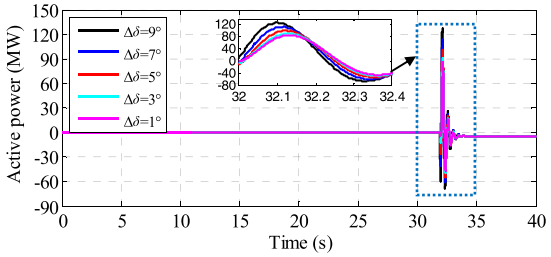

FIGURE 19. The active power of synchronous condenser.

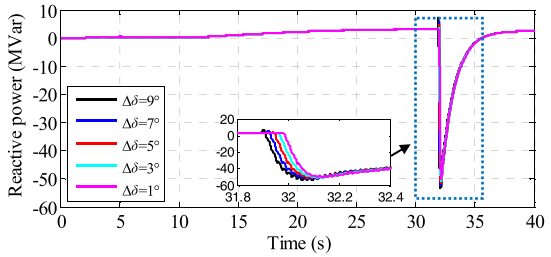

FIGURE 20. The reactive power of synchronous condenser.

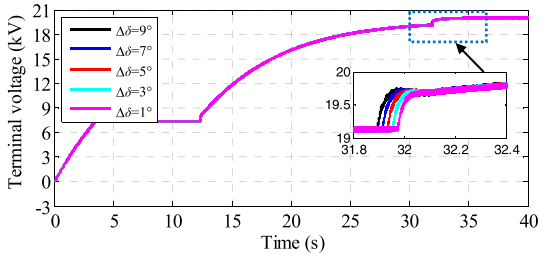

FIGURE 21. The terminal voltage of synchronous condenser.

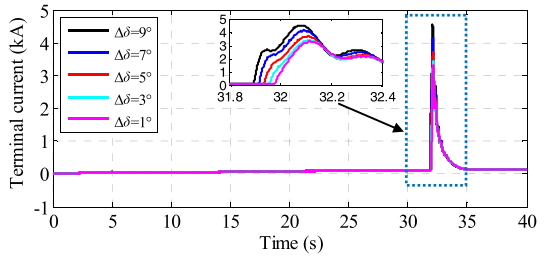

FIGURE 22. The terminal current of synchronous condenser.

The surges of active powers of SC with different phase differences are shown in Fig. 19. According to theoretical analysis, the surges at the grid integration instant become more significant with a larger setting value of the phase difference. However, if the phase difference is set too small, it may result in a narrow synchronization window, which lead to the failure of grid integration. It can be demonstrated in Fig. 19 that when the phase difference of the SC is set to 9°, the surge of active power is the highest, exceeding 125 MW. It is the smallest when the phase difference is set to 1° with about 85 MW. Compared with the former, the surge is reduced by 32%.

The surges of reactive powers of SC with different phase differences are displayed in Fig. 20. When the phase difference is set to 9°, the surge peak value of reactive power reaches 54 MVar, which is about 36% of the CDPA. While it becomes about 50 MVar when the phase difference is set to 1° with about 33% of the CDPA. Compared with the former, the surge is not significant.

The surges of terminal voltages of SC with different phase differences are shown in Fig. 21. When the phase difference is set to 9°, the voltage difference before/after the grid integration is 0.88kV. While it becomes 0.84 kV when the phase difference is set to 1°. Hence, when the phase difference is set to 1° ∼9°, the terminal voltage difference before/after the grid integration meets the preset value, i.e. the voltage difference meets within 5% of the rated voltage.

The surges of terminal currents of SC with different phase differences are shown in Fig. 22. When the phase difference is set to 1°, the surge of the terminal current is the lowest, which is about 3.3 kA with only 38% of the rated current. When the phase difference is set to 9°, it will be the highest surge, which exceed 4.7 kA with 54% of the rated current. Compared with the former, the surge increases by 42%.

The simulation results demonstrate that the integration surge is proportion to the phase difference of the SC. In addition, when the phase difference of grid integration is set to 1°, there is no failure of the grid integration for the synchronous condense due to appropriate the preset initial falling speed and the frequency difference. In practical applications, the complex operation and the other interference factors are taken into account, in order to ensure the security and reliability of the grid integration and the control margin of phase difference, the constraint criterion is controlled at 4.5° ∼ 5.5°. According to the analysis and simulation results in Section IV-C, the setting of different phase differences of grid integration has a small impact on reactive power and terminal voltage but a large impact on active power and terminal current. Hence, when the phase difference is set to 5°, the performance of active power and terminal current in Fig. 19 and in Fig. 22 should be emphatically analyzed. It can be shown in Fig. 19 that when the integration phase difference of the SC is set to 5°, the surge of active power is large with exceeding 100 MW. When the phase difference is set to 1°, the surge of active power is about 85 MW. The difference of them is 15%. Fig. 22 shows that when the integration phase difference of the SC is set to 5°, the surge of terminal current exceeds 3.7 kA. When the phase difference is set to 1°, the surge of terminal current is about 3.3 kA. The difference of them is 12%, which is a large difference in both active power and terminal current.

V. ANALYSIS AND DISCUSSION

This paper has focused on the analysis of the performance of SC with VSC-based SFC under three different grid integration constraint criterions, including initial falling speeds, frequency differences and phase differences. This paper has identified the impact on the dynamic behaviors under

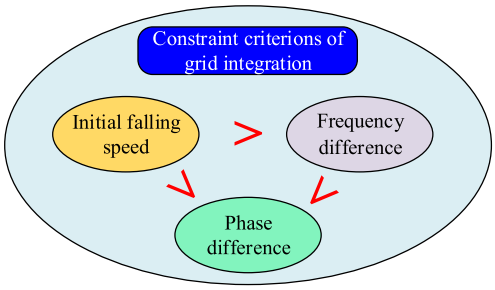

FIGURE 23. Game diagram of grid integration constraint criterions of synchronous condenser.

different criterions of grid integration constraint for the SC and the game relationship between them. The game diagram of the grid integration constraint criterions is shown in Fig. 23.

- Analysis in Section IV-A indicates that if the initial falling speed is set to 1.03 times of the rated speed or less, the surges of reactive power and terminal voltage/current will exceed the preset value. In practical application, it will inevitably lead to relay protection operation of SC and then failure of grid integration. Thus, in comparison with the optimized initial falling speed (1.05 times of the rated speed), when the error value of the initial falling speed exceeds 2%, it may lead to the failure of grid integration of the SC.
- Section IV-B presents that when the frequency difference is set to 0.2 Hz or less, the synchronization integration window has more significant narrow to capture the appropriate synchronization integration point, and thereby the failure of grid integration. Therefore, in comparison with the optimized frequency difference (0.4 Hz), when the error of frequency difference exceeds 50% which leads to a failure of integration of SC.
- Section IV-C demonstrates that even if the phase difference is set to 1° or 9°, the SC can capture the appropriate synchronization integration point with a surge peak value not exceeding the preset value. Hence, compared with the optimized phase difference (5°), when the error of phase difference is within 80%, it will not result in the failure of grid integration.

According to the theoretical analysis and simulation results, it can be analyzed that the game relationship of the three different criterions of grid integration constraint is that the inflation on the surge of initial falling speed is the largest, the frequency difference surge is the second, and the phase difference is the smallest. Hence, when evaluating the optimization setting of the constraint criterions, the initial falling speed setting must be strictly controlled, the frequency difference setting can be appropriately optimized within the preset value range, and the phase difference setting can be optimized in a large margin. Finally, the optimized criterions of grid integration constraint will be achieved without failure of grid integration. The analysis and discussion is essential for the design of control system and the setting of constraint criterions at the SC.

VI. CONCLUSION

In this paper, the start-up control and grid integration characteristics of a 300 MVar SC using VSC-based SFC has been investigated in this paper. The topological structure and control strategy of the VSC-based SFC have been proposed. A mathematical model of the SFC-based SC has been established. Dynamic behaviors of interconnected system during the start-up period with three different criterions of grid integration constraint for the SC, including initial falling speed, frequency difference and phase difference, have been analyzed. A comprehensive starting control strategy of the SC with optimized initial falling speed, optimized frequency difference and optimized phase difference has been proposed based on the theoretical analysis and simulation experiments.

- When the initial falling speed of SC is set to 1.03 times of the rated speed or below, the grid integration will fail. When it is 1.05 times rated speed, the grid integration surge will be the smallest. Hence, the error range of initial falling speed is 2%.
- When the frequency difference of SC is 0.2 Hz or less, and thereby failure of the grid integration. When 0.4 Hz is used as the frequency difference, the grid integration surge will be the smallest. Hence, the error range of frequency difference is 50%.
- When the phase difference of SC is set to 1° or 9°, the appropriate synchronization integration instant can be achieved, and the peak value will not exceed the preset value. Compared with the optimized grid synchronization phase difference (5°), the error range of phase difference is 80%.

According to the theoretical analysis and simulation results, in order to ensure the security and reliability of grid integration and control margin of the three constraint criterions. The initial falling speed has been proposed to be set as 1.05 times of the rated speed, the frequency difference range to be controlled at 0.4 Hz $\sim$ 0.5 Hz and the phase difference range to be controlled at 4.5° $\sim$ 5.5°. The simulation model established in PSCAD/EMTDCTM can provide an effective verification platform for practical applications and data analysis of a SC integrated power grid under different criterions of grid integration constraint.

Variable frequency starting control with the VSC-based SFC or CSC-based SFC has been proposed, which can increase the rotor speed of SC. It is connected into the system by the integration circuit breaker when it goes into falling speed operating condition. In practical applications, a VSC-based SFC is often used to start a small or medium capacity SC and a CSC-based SFC is used to start the large-capacity SC. With the constant upgrade and innovation of power electronic devices, the actual application of starting the large-capacity SCs with VSC-based SFC under variable frequency control mode is inevitable in the future for the advantages of fully-control power electronics devices. This paper has done more in-depth and prospective study in this direction. The AC terminal voltage of the SCs has been gradually increased by

variable frequency starting control. A stable rise of the rotor speed has been achieved and the surges of grid integration has been effectively reduced during the falling speed operation. The grid integration process is consistent with the practical application. Hence, high reliability theoretical support has been provided for the grid integration of the SCs. This paper has focused on the modes of grid integration and the performance of the large-capacity SCs started with the VSC-based SFC. The start-up control with CSC-based SFC will be proposed, and compare and analyze it with the research of this paper. The new generation large-capacity SCs will definitely play an important role in power grid in the future for its unique advantages.

REFERENCES

[1] Y. Xue, X.-P. Zhang, and C. Yang, "Commutation failure elimination of LCC HVDC systems using thyristor-based controllable capacitors," *IEEE Trans. Power Del.*, vol. 33, no. 3, pp. 1448–1458, Jun. 2018.

[2] S. Gao, Q. Liu, and G.-B. Song, "Current differential protection principle of HVDC transmission system," *IET Gener., Transmiss. Distrib.*, vol. 11, no. 5, pp. 1286–1292, Mar. 2017.

[3] C. Zou, H. Rao, S. Xu, Y. Li, W. Li, J. Chen, X. Zhao, Y. Yang, and B. Lei, "Analysis of resonance between a VSC-HVDC converter and the AC grid," in *Proc. IEEE Trans. Power Electron.*, vol. 33, no. 12, pp. 10157–10168, Dec. 2018.

[4] Z. Liu, X. Qin, Q. Zhao, and L. Zhao, "Study on the application of UHVDC hierarchical connection mode to multi-infeed HVDC system," *Proc. CSEE*, vol. 33, no. 10, pp. 1–7, 2013.

[5] T. H. Nguyen, D.-C. Lee, and C.-K. Kim, "A series-connected topology of a diode rectifier and a voltage-source converter for an HVDC transmission system," *IEEE Trans. Power Electron.*, vol. 29, no. 4, pp. 1579–1584, Apr. 2014.

[6] Y. Gao and M. X. Han, "Steady state characteristic of multi-infeed UHVDC power transmission," *Power Syst. Technol.*, vol. 38, no. 12, pp. 3447–3452, Dec. 2014.

[7] Y. Wang, Y. Zhang, Q. Zou, and Z. Q. Li, "Study on application of new generation large capacity synchronous condenser in power grid," *Power Syst. Technol.*, vol. 41, no. 1, pp. 22–28, Dec. 2017.

[8] J. Tu, Y. Pan, J. Zhang, B. Zeng, J. Jia, and J. Yi, "Transient reactive power characteristics of HVDC during commutation failure and impact of HVDC control parameters," *J. Eng.*, vol. 2017, no. 13, pp. 1134–1139, Nov. 2017.

[9] F. Shixiong, H. Wei, L. Lixin, W. Wei, Z. Peng, F. Jiayu, H. Yiping, and X. Guorui, "Influence of synchronous condenser exciter limit on voltage stability of HVDC," in *Proc. IEEE Int. 13th Conf. Ind. Electron. Appl.*, May/Jun. 2018, pp. 210–215.

[10] T. Petersson and K. Frank, "Starting of large synchronous motor using static frequency converter," *IEEE Trans. Power App. Syst.*, vol. PAS-91, no. 1, pp. 172–179, Jan. 1972.

[11] A. H. Taguchi, B. S. Tamai, C. Y. Hosokawa, and D. A. Ando, "APS control method for gas turbine start-up by SFC," in *Proc. Int. Power Electron. Conf.*, Kobe, Japan, 2010, pp. 264–269.

[12] H. Huang and X. Chu, "Improving rotational inertia of power system with variable speed synchronous condenser," in *Proc. IEEE Power Energy Soc. Gen. Meeting*, Chicago, IL, USA, Jul. 2017, pp. 1–5.

[13] W. Chandrasena, B. Bisewski, and J. Carrara, "Effects of phase-shifting transformers and synchronous condensers on breaker transient recovery voltages," *Electr. Power Syst. Res.*, vol. 79, no. 3, pp. 466–473, Mar. 2009.

[14] Q. Wang, J. B. Sha, P. C. Yang, C. Y. Zhao, and D. H. Xu, "Research on the influence of synchronous condenser on LCC-HVDC commutation failure resilience," (in Chinese), *Adv. Tech. Electr. Eng. Energy*, vol. 37, no. 5, pp. 29–36, 2018.

[15] H. T. Nguyen, G. Yang, A. H. Nielsen, and P. H. Jensen, "Combination of synchronous condenser and synthetic inertia for frequency stability enhancement in low inertia systems," *Trans. Sustain. Energy*, vol. 10, no. 3, pp. 997–1005, Jul. 2019.

[16] J. Jia, G. Yang, A. H. Nielsen, and V. Gevorgian, "Investigation on the combined effect of VSC-based sources and synchronous condensers under grid unbalanced faults," *IEEE Trans. Power Del.*, vol. 34, no. 5, pp. 1898–1908, Oct. 2019.

[17] A. Aamir, L. Qiao, C. Guo, A. U. Rehman, and Z. Z. Yang, "Impact of synchronous condenser on the dynamic behavior of LCC-based UHVDC system hierarchically connected to AC system," *CSEE J. Power Energy Syst.*, vol. 5, no. 2, pp. 190–198, Jun. 2019.

[18] Y. Ma, L. Ruan, Y. Xiao, L. Zhou, J. Wang, and Q. Tao, "Modelling and analysis of the UHVDC transmission receiving system considering 300 Mvar novel synchronous condenser," *J. Eng.*, vol. 2019, no. 16, pp. 955–960, Apr. 2019.

[19] Y. Ma, Z. Ling, W. Cai, Y. Cui, L. Zhou, and J. Wang, "A novel coast-down no-load characteristic test and curve conversion method for large-scale synchronous condenser," *Elect. Power Syst. Res.*, vol. 172, pp. 77–85, Jul. 2019.

[20] X. Wang, P. Zou, Y. Wang, and Z. Q. Li, "Bushing PD analysis and electric field simulation large capacity synchronous compensator," (in Chinese), *Elect. Eng.*, vol. 23, no. 10, pp. 31–35, 2016.

[21] Y. Zhang and A. M. Gole, "Comparison of the transient performance of STATCOM and synchronous condenser at HVDC converter stations," in *Proc. IET Int. Conf. AC DC Power Trans.*, Birmingham, U.K., 2015, pp. 1–8.

[22] F. Xiao, Y. B. Zhou, L. Ruan, K. P. Zhou, T. Wang, K. Cao, and Y. Z. Rao, "Study on transient reactive power characteristics of new-generation large synchronous condenser," in *Proc. China Int. Conf. Elect. Distr. (CICED)*, Sep. 2018.

[23] H.-S. Ryu, B.-S. Kim, J.-H. Lee, and I.-H. Lim, "A study of synchronous motor drive using static frequency converter," in *Proc. 12th Int. Power Electron. Motion Control Conf.*, Aug./Sep. 2009, pp. 1496–1499.

[24] J. Le, and R. X. Hu, *Circuit Design and Simulation of PSCAD*, 4nd ed. Beijing, China: Mechanical Industry Press, 2015, pp. 139–148.

[25] X. Z. Tang, R. Dang, Y. D. Liu, L. Shi, K. Wang, and P. Y. Wang, "Control strategy for voltage stabilization of HVDC transmission system with integration of a synchronous condenser," *Proc. CSU-EPSA*, vol. 31, no. 1, pp. 65–70, Jan. 2019.

[26] B. T. Ooi and R. A. David, "Induction-generator/synchronous-condenser system for wind-turbine power," *Proc. Ins. Electr. Eng.*, vol. 126, no. 1, pp. 69–74, Jan. 1979.

[27] G. Magsaysay, T. Schuette, and R. J. Fostiak, "Use of a static frequency converter for rapid load response in pumped-storage plants," *IEEE Trans. Energy Convers.*, vol. 10, no. 4, pp. 694–699, Dec. 1995.

[28] N. Mendis, K. M. Muttaqi, and S. Perera, "Management of battery-supercapacitor hybrid energy storage and synchronous condenser for isolated operation of PMSG based variable-speed wind turbine generating systems," *IEEE Trans. Smart Grid*, vol. 5, no. 2, pp. 944–953, Mar. 2014.

[29] D. Tao, B. Ge, P. Lin, and C. Dong, "Harmonics characteristics of generator/motor starting with static frequency converter during low frequency," *Proc. CSEE*, vol. 34, no. 36, pp. 6450–6457, Nov. 2014.

[30] C. Yibo, T. Qian, L. Zaixun, C. Wanli, R. Ling, and Y. Pengcheng, "Analysis on design points of large synchronous condenser for UHVDC project," in *Proc. Int. Conf. Syst. Rel. Sci.*, Paris, France, 2017, pp. 12–16.

[31] S. Kalsi, D. Madura, and M. Ross, "Performance of superconductor dynamic synchronous condenser on an electric grid," in *Proc. IEEE Trans. Distr. Conf. Expo.*, Aug. 2005, pp. 1–5.

[32] M. Kim, C. Park, S. Je, H. Jang, C. Joo, and S. Kang, "Real-time compensation of simultaneous errors induced by optical phase difference and substrate motion in scanning beam laser interference lithography system," *IEEE Trans. Mechatronics*, vol. 23, no. 4, pp. 1491–1500, Aug. 2018.

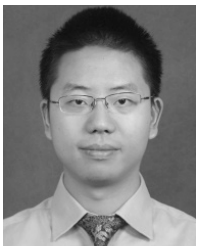

PUYU WANG (S'13–M'15) received B.Eng. degree in electrical engineering from the Huazhong University of Science and Technology (HUST), China, and the B.Eng. degree in electrical engineering and the Ph.D. degree from the University of Birmingham, Birmingham, U.K., in 2011 and 2016, respectively.

From 2013 to 2016, he was a Research Fellow of electrical power systems with the University of Birmingham. He is currently a Lecturer with the Department of Electrical Engineering, School of Automation, Nanjing University of Science and Technology (NUST), China. His research interests include HVDC technology, dc–dc converters, grid integration of renewable energy, and power electronics applications in power systems.

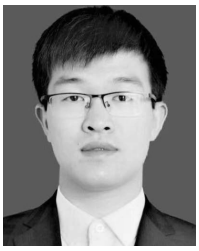

XING LIU is currently pursuing the M.Eng. degree in electrical engineering with the Nanjing University of Science and Technology (NUST), Nanjing, China.

His current research interests include start-up, protection and control of synchronous condensers, and HVDC technologies.

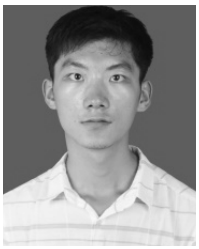

QINGWEN MOU received the B.Eng. degree in electrical engineering from the Nanjing University of Science and Technology (NUST), Nanjing, China, in 2018, where he is currently pursuing the M.Eng. degree.

His research interests include operation, control, and protection of synchronous condensers and HVDC technologies.

WEI GU (M'06–SM'16) received the B.Sc. and Ph.D. degrees in electrical engineering from Southeast University, Nanjing, China, in 2001 and 2006, respectively.

From 2009 to 2010, he was a Visiting Scholar with the Department of Electrical Engineering, Arizona State University, Tempe, AZ, USA. He is currently a Professor with the School of Electrical Engineering, Southeast University. He is the Director of the Institute of Distributed Generations and Active Distribution Networks. His research interests include distributed generations and microgrids, and active distribution networks.

XUEHUA ZHAO received the Ph.D. degree in electrical engineering from the China University of Mining and Technology, China, in 2016.

He is currently an Engineer with State Grid Jiangsu Electric Power Company, Ltd., China. His research interests include HVDC technology, synchronous condensers, and power electronics applications in power systems.